Aerosol and Air Quality Research, 17: 913–922, 2017

ISSN: 1680-8584 print / 2071-1409 online
doi: 10.4209/aaqr.2016.07.0312

High-Performance Amino-Functional Graphene/CNT Aerogel Adsorbent for Formaldehyde Removal from Indoor Air

Jie Ma[1,2], Yiran Sun[1], Jinhu Yang[3], Zichen Lin[1], Qianying Huang[1], Tian Ou[1], Fei Yu[2,4*]

[1] *State Key Laboratory of Pollution Control and Resource Reuse, College of Environmental Science and Engineering, Tongji University, Shanghai 200092, China*
[2] *College of Chemistry and Environmental Engineering, Shanghai Institute of Technology, Shanghai 2001418, China*
[3] *School of Chemical Science and Engineering, Tongji University, Shanghai 200092, China*
[4] *Jiangsu Key Laboratory for Environment Functional Materials, Suzhou University of Science and Technology, Suzhou 215009, China*

ABSTRACT

A flexible approach prepares amino-functional graphene aerogels with different additions of carbon nanotubes (CNTs) for use as an adsorbent to study the adsorption performance of formaldehyde in indoor air. Experimental results indicated that the decoration of amino groups offers a greater number of chemical adsorption sites, which mainly contributed to the improvement of the chemical adsorption capacity of graphene aerogels, and the breakthrough time increased from 0 to 390 min g^{-1} under 3.7 ppm of formaldehyde. The addition of CNTs can significantly enhance the adsorption properties. More interestingly, the breakthrough time presents a substantial increase from 390 to 20,300 min g^{-1} when the mass ratio of CNTs and graphene increased from 0:1 to 2:1 and then decreased to 18,000 min g^{-1} at the ratio of 3:1. The addition of CNTs weakens the agglomeration degree and achieves a greater number of adsorption sites by playing a supportive and connective role among graphene sheets. However, more CNTs will agglomerate, and fewer functional groups on the surface limit additional amounts. The adsorption mechanism was also studied by analyzing the surface specific area and N content. This work provides new insights into the application of amino-functional graphene aerogels with the additions of CNTs (AGCAs) as a potential adsorbent to eliminate indoor formaldehyde pollution.

Keywords: Graphene; Carbon nanotube; Aerogel; Adsorbent; Formaldehyde.

INTRODUCTION

Indoor air quality is of great importance for human health because people spend more than 80% of their time in offices, cars, houses and schools. "Sick building syndrome" in new houses has become a major issue with the increase in indoor air pollutants (Yu and Crump, 1998). Formaldehyde (HCHO) emitted from construction and decoration materials is regarded as one of the most dominant and harmful indoor volatile organic compounds (VOCs) (Salthammer *et al*., 2010). Salonen *et al*. (2009) showed that formaldehyde is more efficient than common volatile organic gas mixtures in stimulating sensory organs. Formaldehyde is listed as a well-known human carcinogen (IARC, 1985). It is a strong irritant to the human sensory and respiratory system, and long-term exposure to HCHO at concentrations as low as 0.03 ppm can lead to tears, breathing difficulties and other symptoms such as headache, nausea, rhinitis, emphysema, and lung cancer (Cogliano *et al*., 2005; Salthammer *et al*., 2010). HCHO has severe impacts on children, which can easily cause asthma (McGwin Jr *et al*., 2010). Research conducted by Paustenbach *et al*. (1997) showed that volunteers suffered eye and respiratory discomfort under formaldehyde concentrations of 0.25–3.0 ppm, and the degree of stimulation of human eyes caused by formaldehyde gas in the range of 0.5–3.0 ppm presents a linear growth trend. Therefore, for the sake of improving indoor air quality and reducing public health risks, it is essential to develop more efficient and environmentally friendly approaches for the elimination of formaldehyde pollution.

Considerable efforts have been made to develop approaches for HCHO removal to meet rigorous environmental regulations. In general, researchers have focused on four main technologies for HCHO removal: adsorption (Pei and Zhang, 2011; Xu *et al*., 2013), photocatalytic oxidation (Yang *et al*., 2000), thermal catalytic oxidation (Chen *et al*., 2011), and plasma technology (Zhao *et al*., 2011). As an approach that is environmentally benign, efficient and conserves energy, adsorption is receiving increased attention.

* Corresponding author.
E-mail address: fyu@vip.163.com

It is known that specific surface area (SSA), porosity and surface functional groups of adsorbents are crucial factors for adsorption properties (Lee *et al*., 2013). There are two major efforts that can be made to improve the adsorption performance of HCHO. The first is to modify adsorbents with different chemical functional groups aimed at improving the reaction of HCHO and functional groups on the material surface. Tanada *et al*. (1999) certified that the presence of nitrogen on a carbon surface is beneficial to the adsorption of formaldehyde. Rong *et al*. (2010) also showed that the adsorption capacity and breakthrough time of formaldehyde were significantly increased in an experiment using an active carbon fibers containing amino groups. Therefore, in virtue of the reaction between amino groups and HCHO, adsorption performance could be significantly improved by modifying adsorbents with amino groups. Moreover, the latter effort can increase the number of physical adsorption sites by increasing SSA and porosity, which can be achieved by selecting different materials and adjusting the preparation technology. Currently, many studies have been carried out on HCHO removal via carbon adsorbents, such as activated carbon, graphene, CNTs, etc. Activated carbon is the most widely used adsorbent, but its efficiency is not optimal due to its limited adsorption capacity. Pei and Zhang (2011) put activation treatment on commercial activated carbon, but the adsorption capacity under 2.36 ppm of formaldehyde was only 0.36 mg g^{-1}. Compared with activated carbon, graphene has exceptional properties of chemical inertness, high thermal conductivity (Geim and Kim, 2008), and mechanical properties (Li *et al*., 2011), which makes graphene easy to functionalize (Elias *et al*., 2009). These features make graphene a promising material for the application of adsorption of formaldehyde. In a previous study, we studied the formaldehyde removal ability of amino-functional graphene-sponge composites decorated by graphene nanodots and achieved a breakthrough time of approximately 2,137 min g^{-1}, presenting a significant improvement in adsorption performance (Wu *et al*., 2015). CNTs have also been widely used for the removal of gaseous and water pollutants (Di *et al*., 2004; Agnihotri *et al*., 2005; Yu *et al*., 2014). Carbon nanotubes (CNTs) have a clearer and more uniform atomic structure because of their special atomic arrangement, diameter, and shape, and show superior physical adsorption properties. However, most researchers studying HCHO adsorption on graphene and CNTs have focused on density functional theory calculations and molecular simulation experiments. Moreover, almost all the adsorbents are applied in the form of particles or powders, which significantly restricts their development due to the nonnegligible aggregation of nanoparticles and difficulties in regeneration and recycling. To address these drawbacks, 3D macroscopic nanomaterials were taken into consideration. The merits of 3D macroscopic nanomaterials are that the 3D structures avoid aggregation, and invalid stack and macroscopic structures reduce the difficulty in separation and recycling of powder-like materials. In particular, the interconnection of space structures maintains or strengthens the performance of carbon nanomaterials (Jo *et al*., 2015).

However, to the best of our knowledge, most studies of 3D macroscopic nanomaterials concentrate on the removal of water-borne contaminants, such as heavy metals, antibiotics, and dyes. Only a few studies have investigated the application of 3D macroscopic nanomaterials on the adsorption of indoor gaseous pollutants. Moreover, the research of amino-group decoration has been primarily directed at activated carbon, and studies on emerging carbon materials are rare.

In this paper, we first report that ACGAs were chosen as adsorbents for HCHO removal from indoor air. An amino-functional graphene aerogel with CNT composites was synthesized, characterized, and analyzed to study how adsorption performance was influenced by amino-group decoration and different additional amounts of CNTs. We observed that the modification can significantly increase the chemical adsorption capacity; CNTs can improve the microstructure of graphene aerogel, and the material exhibited the greatest adsorption capacity when performed under the proper ratio of graphene and CNTs.

EXPERIMENTAL

Materials

All chemicals used in this research, including polyoxymethylene, ethylenediamine (EDA), and ammonium hydroxide, were purchased from Sinopharm Group Co. (Shanghai, China) and were of analytical grade and used directly without purification.

Preparation of Graphene Aerogel (GA)

The graphene oxide (GO) was prepared using a modified Hummer's method (Hirata *et al*., 2004), dispersed in deionized water and sonicated in an ultrasound bath for 6 h to obtain a GO aqueous dispersion (1.0 mg mL^{-1}). The graphene aerogel (GA) was prepared by hydrothermal reduction using ascorbic acid (VC) as the reducing agent. Then, 150 mg of ascorbic acid was added to the GO solution to obtain a mass ratio of 1:1 and followed by ultrasonic dispersion for 15 min to dissolve the ascorbic acid. Then, the solution was sealed in a glass vial and placed into a water bath of 95°C for 12 h to form hydrogel. Finally, the hydrogel was turned into the aerogel G1N0 (VC) using a freeze-drying method after soaking and washing in deionized water.

Preparation of Carbon Nanotubes (CNTs)

The CNTs were prepared by a catalytic chemical vapor deposition method (Ma *et al*., 2009). Precisely 1 g of ferrocene and 1 mL of thiophene were dissolved in 100 mL of ethanol for the preparation of a solution with different concentrations of ferrocene and thiophene, in which ethanol serves as the carbon feedstock, ferrocene as the catalyst and thiophene as a growth promoter. The solution was sonicated for 10 min and then transferred to a pyrolysis spray storage mainly composed of a tubular furnace that had a heating length of 70 cm and a quartz tube heated to 1100°C. During the temperature increase, N_2 flow was initiated in the quartz tube to eliminate oxygen from the reaction chamber. After 15 min of maintaining the desired temperature, a solution dissolved with ferrocene and thiophene was supplied by an

electronic micropump at a rate of 0.2 mL h^{-1} and sprayed through a nozzle with a N_2 flow of 60 mL h^{-1}.

Preparation of Amino-Functional Graphene/CNTs Aerogel (AGCA)

The amino graphene/CNTs aerogel (AGCA) was prepared by hydrothermal reduction using ethylenediamine (EDA) as the reducing agent. A total of 150 mg of uniform GO solution with a concentration of 1 mg mL^{-1} was prepared as previously mentioned, followed by the addition of 1600 μL EDA, 400 μL ammonia (30%) and different amounts of CNTs (0 mg, 75 mg, 150 mg, 300 mg, and 450 mg). Subsequently, the mixture was fully mixed, sealed and heated in a water bath at a constant temperature of 95°C to obtain hydrogels decorated with amino-groups on GO surfaces, which consisted of different proportions of graphene and CNTs (G1N0, G1N0.5, G1N1, G1N2, and G1N3). Finally, the hydrogels were turned into aerogels by a freeze-dried method after soaking and washing in deionized water.

Adsorption Experiment

The schematic of the adsorption experiment is shown in Fig. S1. The test system was mainly composed of three parts. The basement of this system is part of the formaldehyde generator. A dynamic volumetric method was used to obtain standard gaseous formaldehyde without interference from water vapor, for which a container of polyoxymethylene was placed in a water bath at a constant temperature to promote the depolymerization reaction, and nitrogen gas of 99.999% purity flowed at a rate of 200 mL min^{-1} into the generator to obtain gaseous formaldehyde at the specific concentration of 3.7 ppm. The other two parts of the schematic are composed of the adsorption and detector equipment of formaldehyde. A total of 100 mg of prepared adsorbents were imported into the system, and a PPM HTV-m formaldehyde analysis instrument (PPM Technology Ltd, UK) was placed at the end of the system.

Breakthrough time is defined as the period when the formaldehyde concentration decreases after reaching the adsorption column and rises to the safety threshold according to guidelines from the WHO (0.08 ppm). The adsorption experiment ends when the output concentration (C) of formaldehyde reaches 80% of the inlet value (C_0). Another critical parameter for judging the adsorption performance of adsorbents is adsorptive capacity (W). The amount of pollutants adsorbed was calculated according to the following equation:

$$W = \frac{P \times M}{R \times T} \times L \times t \times 10^6 \quad (1)$$

P is the atmospheric pressure (Pa).
M is the mole weight of formaldehyde (30.01 g mol^{-1}).
R is the ideal gas constant (8.314 $J.K^{-1}$ mol^{-1}).
T is the Kelvin temperature (K).
L is the volume flow rate of nitrogen (L min^{-1}).
t is the breakthrough time of adsorbent samples in the experiments (min g^{-1}).

Characterization Method

The microstructure and morphology of the aerogels were analyzed by scanning electron microscopy (SEM, JSM-6400F, Japan). Fourier transform infrared spectra (FT-IR) of powder samples were recorded on a Tensor 27 FTIR spectrometer (Bruker Optics, Inc.). X-Ray photoelectron spectroscopy (XPS) analysis was carried out on a Kratos Axis Ultra DLD spectrometer using monochromated Al Ka X-rays at a base pressure of 1×10^{-9} Torr. Survey scans between 1100 and 0 eV were performed to determine the overall elemental composition of the sample, and regional scans were conducted for specific elements. The peak energies were calibrated by placing the major C1s peak at 284.6 eV. Samples were prepared identically to those of the batch experiments. N_2 adsorption experiments using an automatic specific surface area/pore size distribution measurement system (BELSORP-mini II, BEL Japan, Inc., Japan) were conducted to investigate the porosity of MWCNTs. All samples were outgassed at 200°C in a nitrogen flow for 4 h before measurement. Nitrogen adsorption data were recorded at the temperature of liquid nitrogen (77 K).

RESULTS AND DISCUSSION

Characterization of Graphene Aerogel Adsorbents

Fig. 1 shows the photographs of graphene hydrogel and aerogel. We can observe that the structure of the hydrogel was well preserved after the freeze-drying process. Additionally, the mechanical strength of graphene aerogel decreases with an increase in the proportion of CNTs (Fig. S2). The surface morphology and microstructures of graphene aerogels are shown in Figs. 1(c)–1(g). Figs. 1(c)–1(e) shows the low-resolution SEM images of G1N0 (VC), G1N0, and G1N1, respectively. The SEM images of G1N0 (VC) in Fig. 1(c) exhibits a three-dimensional interconnected structure consisting of graphene sheets. Compared with G1N0 (VC), the SEM images of G1N0 in Fig. 1(d) show a more obvious network structure with more pores. We attribute this distinction to the addition of amino groups in G1N0. Considering the formation of G1N0, graphene sheets were reduced and modified with amino groups, which contribute to the network and pore structures. Comparing the SEM images of G1N0 and G1N1, with the addition of CNTs, G1N1 presents a more regular and compact network. We infer that CNTs have an effect on the combination of graphene sheets and results in a more compact network.

The high-resolution TEM images (Figs. 1(e) and 1(f)) show the three-dimensional structure of graphene aerogels formed by the wrinkling and stacking of single- or few-layer graphene sheets. CNTs are observed clearly in Fig. 1 g and are distributed uniformly among the graphene sheets. When comparing the TEM images of G1N0 and G1N1, the graphene sheets in G1N0 agglomerate to some extent, whereas the addition of CNTs decreases the agglomeration degree by supporting and connecting the graphene sheets.

The nitrogen (77.4 K) adsorption-desorption plots and pore-size distribution (PSD) of the graphene aerogels are shown in Figs. 2 and 3, respectively. The specific surface area (SSA) and pore structure parameters of the samples

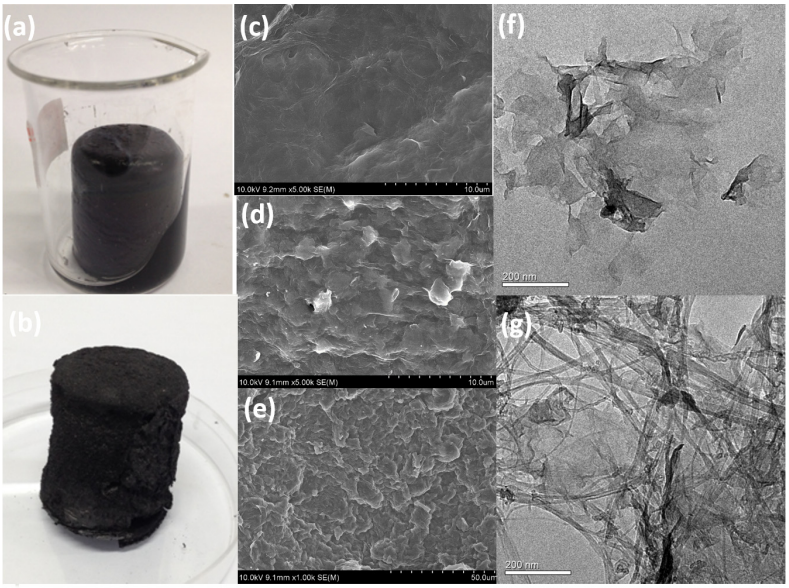

Fig. 1. Optical images of amino-functional graphene hydrogel (a) and amino-functional graphene/CNTs aerogel (b); SEM images of G1N0 (VC) (c), G1N0 (d), G1N1 (e), TEM images of G1N0 (f) and G1N1 (g).

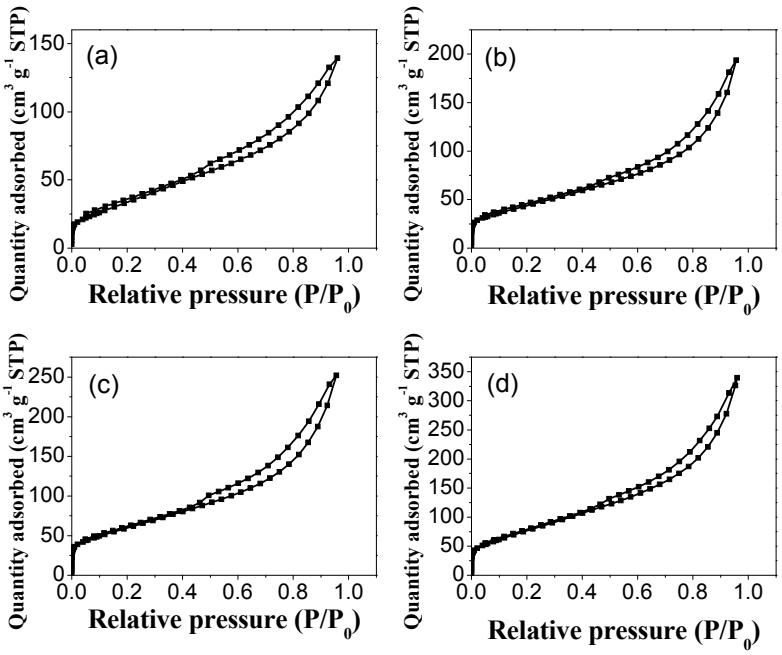

Fig. 2. N_2 adsorption-desorption isotherm of G1N0.5 (a), G1N1 (b), G1N2 (c), and G1N3 (d).

are summarized in Table 1. As shown in Table 1, with the addition of CNTs, the SSA and pore volume of G1N2 (VC) are significantly greater in comparison to those of G1N0 (VC). This result is in accordance with the conclusion obtained from the SEM image analysis, which concludes that the addition of CNTs results in a variation of structure and microtopography in graphene aerogel. The N_2 isotherms are fitted to a type H3 isotherm (Thommes *et al*., 2015). Loops of this type are typically formed by non-rigid aggregates of plate-like particles (e.g., certain clays) but can also be found if the pore network consists of macropores that are not completely filled with pore condensate. The influence of the additional amount of CNTs on the graphene aerogel can also be observed. G1N0.5 has an SSA of approximately 136.7 $m^2 g^{-1}$, and there is an obvious increase to 287.2 $m^2 g^{-1}$ (G1N3) with an increase in the added amount of CNTs. This trend is also reflected in the variation of pore volumes from 0.194 to 0.473 $cm^3 g^{-1}$ (BJH). Despite a few large pores, the majority of pore sizes are narrowly distributed at approximately 2 nm (Fig. 3), indicating that micropores also exist in the aerogel samples. In addition, when the ratio of CNTs increase, the number of micropores also increase. This implies that CNTs in graphene aerogel contributed to the resistance of aggregation between graphene sheets.

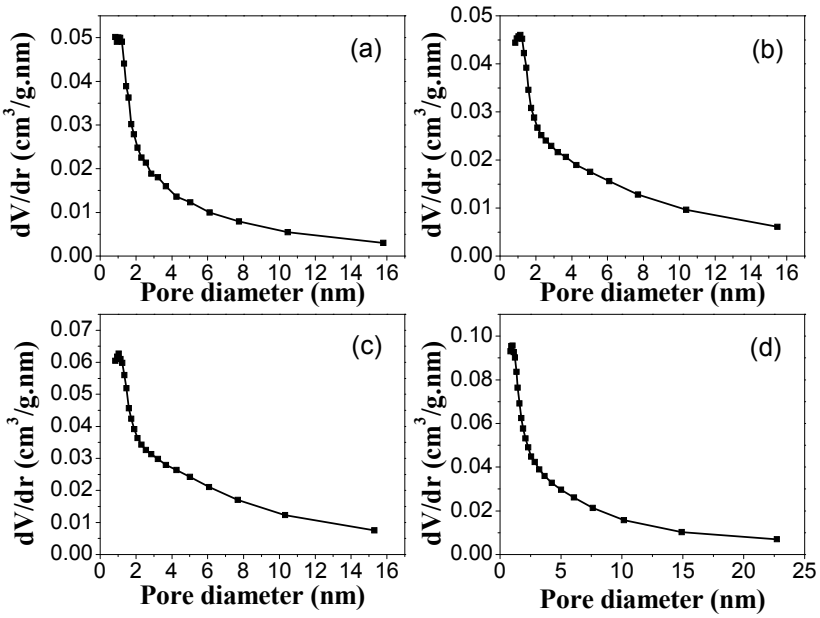

Fig. 3. Pore size distributions of G1N0.5 (a), G1N1 (b), G1N2 (c), and G1N3 (d) by original density functional theory.

Table 1. The specific surface area and pore structures of graphene aerogels.

Samples	Surface area ($m^2 g^{-1}$)[a,c]	Pore volume ($cm^3 g^{-1}$)[a,b]	Average pore size (nm)[a,b]
G1(VC)	262.4	0.309	2.5
G1N2(VC)	273.4	0.504	3.69
G1N0.5	136.7	0.194	2.97
G1N1	161.2	0.268	3.66
G1N2	219.7	0.345	3.54
G1N3	287.2	0.473	3.42

a Properties determined with a gas sorption analyzer.
b Calculated by using the Barret–Joyner–Hallender (BJH) Model.
c Calculated by using the Brunauer–Emmett–Teller (BET) equation.

The FTIR curves for G1N0 (VC), G1N0, and G1N2 are shown in Fig. 4. G1N0 (VC) has been identified with the following functional groups: the strong peak at approximately 3400 cm^{-1} is attributed to the stretching vibration of –OH (Davis *et al*., 1999), the peak at 1618 cm^{-1} corresponds to the stretching vibration of the benzene ring C=C (Daifullah and Girgis, 2003; Ma *et al*., 2012), and the peaks at 918 and 1198 cm^{-1} correspond to the stretching vibrations of the alkoxy C-O and C-OH bonds, respectively (Gu *et al*., 2015). The IR spectrum of G1N0 shows a similar intensity for the –OH peak at approximately 3400 cm^{-1} when compared to the spectrum of G1N0 (VC), which indicates that GO has been reduced to a similar degree by VC and EDA. Instead, the disappearance of the peaks at 918 and 1198 cm^{-1} in G1N0 and the corresponding appearance of a broad peak with lower frequency at 1,122 cm^{-1}, which has been ascribed to the stretch vibrations of the C-N bond (Mawhinney *et al*., 2000; Ramanathan *et al*., 2005), indicates that the graphene aerogel was successfully decorated by amino groups in the reduction process by EDA. In comparison to G1N0, the peak at approximately 3400 cm^{-1} in G1N2 was significantly weakened. It is reasonable to conclude that the difference is due to the addition of CNTs. CNTs are more hydrophobic because they have fewer oxygen-containing functional groups, which are adsorption sites for polar water molecules.

To further investigate and elucidate the variation of chemical bonds and elements on the graphene aerogel surfaces, XPS analyses were performed. The obtained survey spectra of GO, G1N0 (VC), G1N0 and G1N2 are summarized in Fig. 5. Peak locations and areas in relation to specific binding energies were determined through the analysis of the raw XPS data. As shown in Fig. 5(a), the peak intensity of O1s in GO is much stronger than others, indicating that many oxygen-containing functional groups in the graphene sheets are removed in the reduction process. Additionally, the presence of N1s (399.08 eV) in the graphene aerogel reduced by EDA revealed that the material has been decorated by amino groups (Hu *et al*., 2013). The N1s peak was further analyzed in Fig. 5(b), which shows that the higher binding energies at 399.5 and 400.4 eV are attributed to the -C-N-H and N-H/-NH_2, respectively. The comparison between C1s in G1N0 and G1N2 is shown in Figs. 5(c) and 5(d). For G1N0, the XPS results show a slight broadening of the C1s peak at 284.3 eV and two other binding energy peaks at 286.1 and 288.3 eV, which were assigned to C-O and the carboxylic acid group, respectively (Ago *et al*., 1999).

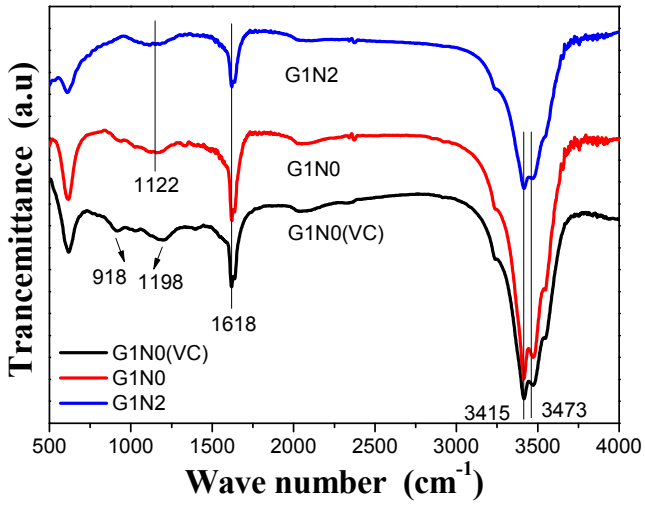

Fig. 4. FTIR spectra of G1N0 (VC), G1N0, and G1N2.

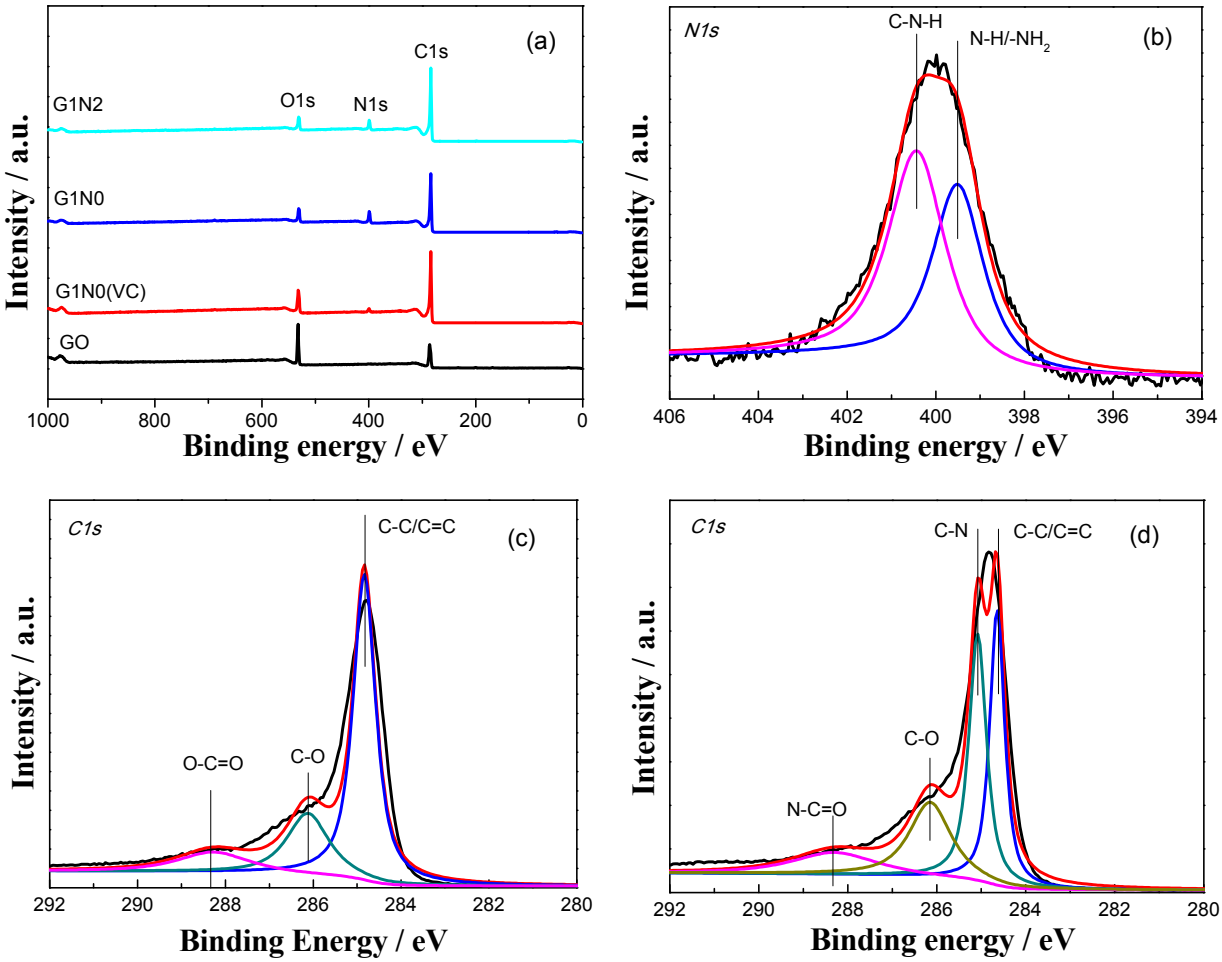

Fig. 5. XPS wide scan (a) of three different aerogels, N1s high-resolution spectra (b) of G1N2, C1s high-resolution spectra (c) of G1N0 (VC), C1s high-resolution spectra (d) of G1N2.

Fig. 5(d) shows the C1s peak of G1N2, which has its main C-C bond at 284.6 eV. The spectrum, however, shows the appearance of two new peaks that were not observed in Fig. 5(c), in which one is the C-N bond at 285.1 eV and the other is the N-C=O bond at 288.3 eV.

These results also confirmed the reaction mechanism of EDA and graphene sheets. The independent electron pair in the nitrogen atom makes EDA nucleophilic. Thus, amino

groups can attract electrons from the aromatic ring and carry out electron donor-acceptor reactions with the graphene sheets. EDA can open the ring of epoxy groups and form amide and imine groups by reacting with carboxyl and carbonyl groups on the edge of the graphene sheets. As a consequence, the graphene aerogel was successfully decorated by amino groups.

Removal Performance of Formaldehyde on AGCAs

Graphene aerogel samples were then put into the adsorption system to investigate their adsorption performance systematically. The breakthrough curves of G1N0 (VC) and G1N0 are shown in Fig. 6. At the formaldehyde concentration of 3.7 ppm, the output value rises to 0.8 ppm immediately after a decline during the test for G1N0 (VC), providing a low adsorption capacity for formaldehyde. For the amino-functional graphene aerogel G1N0, which has the same preparation process as G1N0 (VC) but with a different reducing agent, a greater adsorption performance with a breakthrough time of 390 min g^{-1} under the same experimental conditions was observed. As shown in Fig. 7, after the modification of amino groups, different amounts of CNTs (0.5 mg mL^{-1}, 1 mg mL^{-1}, 2 mg mL^{-1}, and 3 mg mL^{-1}) were added into the aerogels to achieve a higher adsorption capacity. Compared with G1N0, the formaldehyde removal ability of other aerogels was improved significantly (2,730 min g^{-1}), indicating that the addition of CNTs enhanced the adsorption performance. The breakthrough time (2,730–20,300 min g^{-1}) revealed a rising trend when the additive amount of CNTs increased from 0.5 mg mL^{-1} to 2 mg mL^{-1}. However, the trend reversed and the breakthrough time decreased to 18,000 min g^{-1} when the mass ratio increased to 1:3.

According to the results of the characterization analysis and adsorption experiments of aerogel samples, the modification of amino groups, such as –N-H and $–NH_2$, on the surface of graphene aerogel has been considered as the critical factor for improving adsorption performance. According to the results from XPS, the reduction process introduced by VC did not show any new elements or functional groups. The adsorption of HCHO onto G1N0 (VC) depends mainly on the van der Waals force between the graphene sheets and formaldehyde gas molecules, which belongs to physical adsorption. However, during its reaction with EDA, the graphene sheets were decorated and reduced by the amino groups, which connected with the carboxyl, carbonyl and epoxy groups on the graphene sheets. Amino groups can react with the C=O bonds in HCHO and thus achieve the aim of removing HCHO. Therefore, the graphene aerogels decorated by amino groups can remove HCHO via both chemical adsorption, which is caused by the reaction between amino groups and C=O bonds, and physical adsorption, which is caused by van der Waals forces; However, chemical adsorption is the main contributor to the improvement of adsorption capacity of graphene aerogels.

In the physical adsorption process of HCHO, the key technology is to improve the SSA and pore properties of graphene aerogel, thus increasing the contact area and probability between HCHO and adsorbents. Meanwhile, chemical adsorption mainly depends on the chemical bonds formed between adsorbents and pollutants. Therefore, it is crucial to increase the amount of effective functional groups on the surface of adsorbents. In the context of graphene aerogel, it is important to improve on the decoration of amino groups, SSA, and pore properties on the surface.

In the preparation of graphene aerogels, aggregation between the graphene sheets has a serious impact on the SSA and pore properties of the material and further affects the adsorption performance of HCHO. Equipped with a special tubular nanostructure, CNTs are expected to play a supportive and connective role among graphene sheets, thus weakening the degree of agglomeration and achieving a greater number of adsorption sites, which can be decorated with effective amino groups. Therefore, the addition of CNTs greatly enhances the removal ability of the amino-functional graphene aerogels.

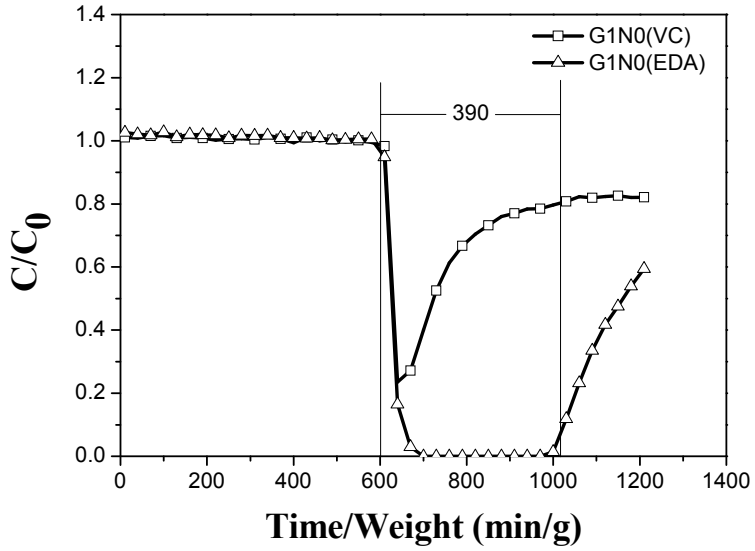

Fig. 6. Breakthrough time of amino-functional aerosols reduced by ascorbic acid and ethylenediamine.

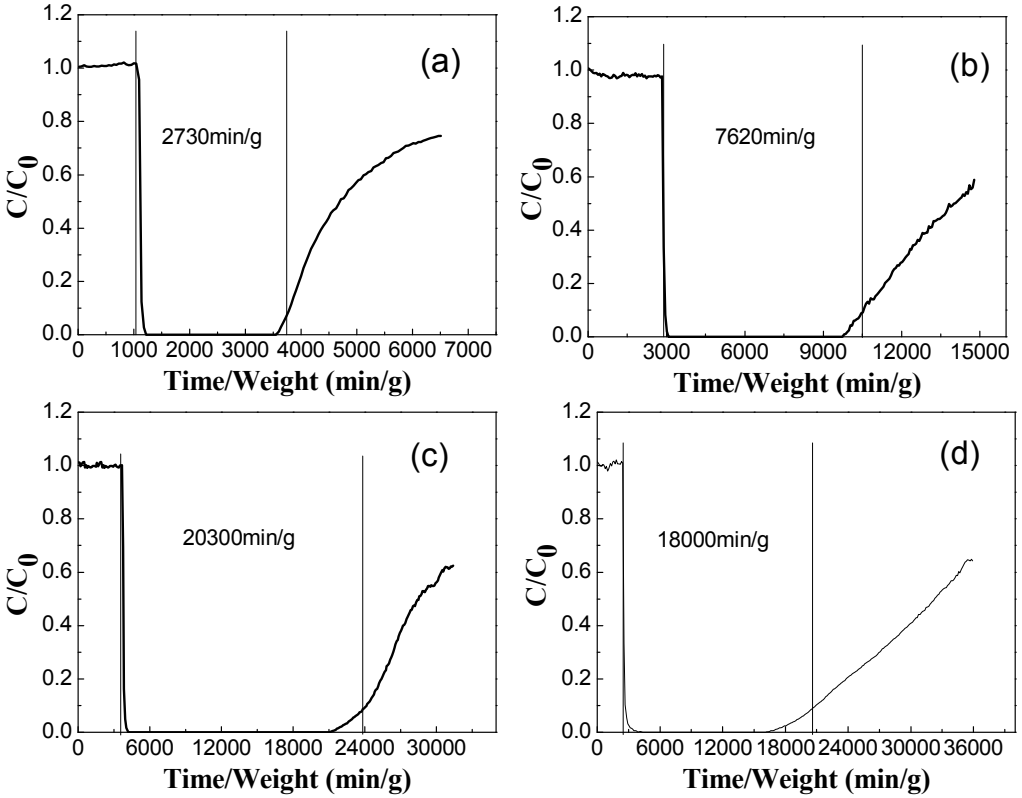

Fig. 7. Breakthrough time of amino-functional aerosols with different additions of CNTs. (a) G1N0.5, (b) G1N1, (c) G1N2, (d) G1N3.

However, CNTs will agglomerate by themselves when the addition of CNTs reaches a certain degree; thus, it is difficult to form a three-dimensional aerogel structure at that time. Moreover, since there is a low amount of functional groups on the walls of CNTs, the difficulty in modification with amino groups weakens the contribution of CNTs in the chemical adsorption of formaldehyde. We inferred that the aspects mentioned earlier were the reasons for the decline of formaldehyde adsorption when the mass ratio of graphene and CNTs reached 1:3.

Removal Mechanism of Formaldehyde on AGCAs

The relationships between the adsorption capacity of gaseous formaldehyde on AGCAs and the ratio of carbon nanotubes, nitrogen content, and specific surface area of aerogels are shown in Fig. 8. For AGCAs, when the proportion of CNTs increases, the specific surface area has a similar growth trend, whereas the atomic content of nitrogen has the opposite trend.

When the added amount of CNTs increases, SSA and pore volume present the same trend, indicating that the addition of CNTs benefits the microstructure and pore properties. However, the contents of elemental N conflict with the amount of CNTs. Since amino groups in graphene aerogels are the main driving force for adsorption of HCHO, an appropriate ratio of CNTs can be recognized as the balance between amino groups and microstructure. Moreover, from Fig. S5, we found that the curvature of the decrease of N content rises with the ratio of CNTs and increases from 0.5 to 3, illustrating that the increase of adsorption sites resulting from the supportive effect of CNTs cannot compensate for the decrease in amino groups. We can infer that the degree of agglomeration increases under a high ratio of CNTs, which destroys the three-dimensional structure. Therefore, when considering the two key factors that affect the adsorption performance of AGCAs, this study demonstrated that the optimal ratio of CNTs is 1:2 and, under these conditions, the adsorption capacity of HCHO onto AGCAs reaches its maximum value.

CONCLUSION

In this study, graphene aerogels were obtained by a feasible hydrothermal reduction method and then used to study their adsorption of HCHO from indoor air. Different reductants were used to investigate the effect of modification with amino-functional groups on the removal of HCHO. We found that the adsorption capacity of graphene aerogels decorated by amino groups was significantly enhanced, since amino groups can offer more chemical adsorption sites, which was the main contributor to the improvement of the chemical adsorption capacity of graphene aerogels. The addition of CNTs weakens the degree of agglomeration and achieves a greater number of adsorption sites by playing a supportive and connective role among graphene sheets. However, when the CNTs content continues to increase, CNTs will agglomerate by themselves, and fewer functional groups on the surface limit the additional amount of

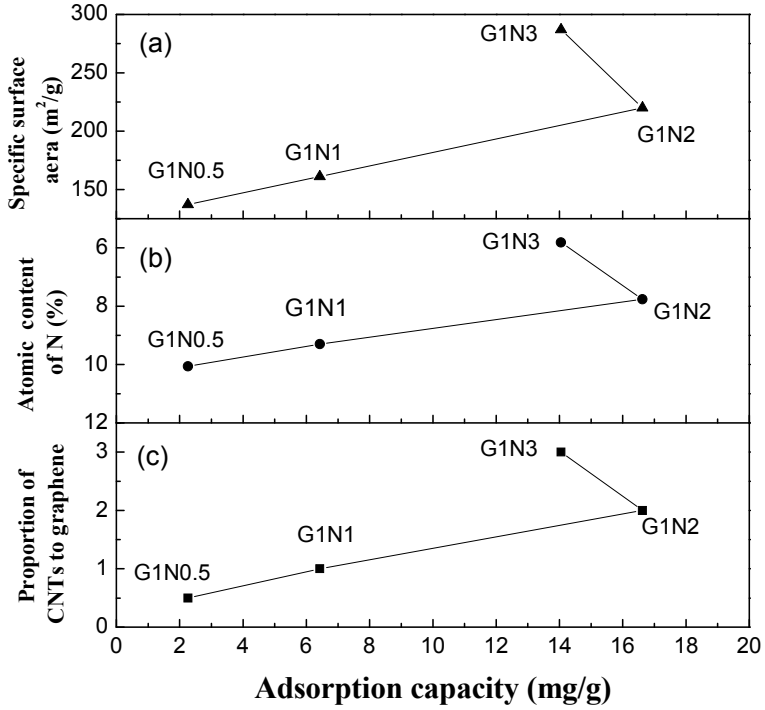

Fig. 8. Variation trends of adsorption capacity with proportion of CNTs, atomic nitrogen content and specific surface area.

adsorption sites. Therefore, when considering the two key factors that affect the adsorption performance of AGCAs, this study demonstrated that the optimal ratio of CNTs is 1:2 and, under these conditions, the adsorption capacity of HCHO onto AGCAs reaches its maximum value. This study provides new insights to develop new applications in the area of 3D nanomaterials. We believe that the outstanding adsorption property of ACGAs is promising in its application to remove HCHO and other indoor pollutants.

ACKNOWLEDGMENT

This research was supported by the National Natural Science Foundation of China (grant nos. 21577099 and 51408362), the State Key Laboratory of Pollution Control and Resource Reuse Foundation (No. PCRRIC16001, No. PCRRF14021), and the Fundamental Research Funds for the Central Universities.

SUPPLEMENTARY MATERIAL

Supplementary data associated with this article can be found in the online version at http://www.aaqr.org.

REFERENCE

Agnihotri, S., Rood, M.J. and Rostam-Abadi, M. (2005). Adsorption equilibrium of organic vapors on single-walled carbon nanotubes. *Carbon* 43: 2379–2388.

Ago, H., Kugler, T., Cacialli, F., Salaneck, W.R., Shaffer, M.S.P., Windle, A.H. and Friend, R.H. (1999). Work functions and surface functional groups of multiwall carbon nanotubes. *J. Phys. Chem. B* 103: 8116–8121.

Chen, D., Qu, Z., Shen, S., Li, X., Shi, Y., Wang, Y., Fu, Q. and Wu, J. (2011). Comparative studies of silver based catalysts supported on different supports for the oxidation of formaldehyde. *Catal. Today* 175: 338–345.

Cogliano, V.J., Grosse, Y., Baan, R.A., Straif, K., Secretan, M.B. and El Ghissassi, F. (2005). Meeting report: summary of IARC monographs on formaldehyde, 2-butoxyethanol, and 1-tert-butoxy-2-propanol. *Environ. Health Perspect.* 113: 1205–1208.

Daifullah, A.A.M. and Girgis, B.S. (2003). Impact of surface characteristics of activated carbon on adsorption of BTEX. *Colloids Surf., A* 214: 181–193.

Davis, W.M., Erickson, C.L., Johnston, C.T., Delfino, J.J. and Porter, J.E. (1999). Quantitative Fourier Transform Infrared spectroscopic investigation of humic substance functional group composition. *Chemosphere* 38: 2913–2928.

Di, Z.C., Li, Y.H., Luan, Z.K. and Liang, J. (2004). Adsorption of chromium (VI) ions from water by carbon nanotubes. *Adsorpt. Sci. Technol.* 22: 467–474.

Elias, D., Nair, R., Mohiuddin, T., Morozov, S., Blake, P., Halsall, M., Ferrari, A., Boukhvalov, D., Katsnelson, M. and Geim, A. (2009). Control of graphene's properties by reversible hydrogenation: Evidence for graphane. *Science* 323: 610–613.

Geim, A.K. and Kim, P. (2008). Carbon wonderland. *Sci. Am.* 298: 90–97.

Gu, Z.X., Wang, Y., Tang, J., Yang, J.J., Liao, J.L., Yang, Y.Y. and Liu, N. (2015). The removal of uranium(VI) from aqueous solution by graphene oxide-carbon nanotubes hybrid aerogels. *J. Radioanal. Nucl. Chem.* 303: 1835–1842.

Hirata, M., Gotou, T., Horiuchi, S., Fujiwara, M. and

Ohba, M. (2004). Thin-film particles of graphite oxide 1:: High-yield synthesis and flexibility of the particles. *Carbon* 42: 2929–2937.

Hu, H., Zhao, Z.B., Wan, W.B., Gogotsi, Y. and Qiu, J.S. (2013). Ultralight and highly compressible graphene aerogels. *Adv. Mater.* 25: 2219–2223.

International Agency for Research on Cancer (IARC) (1985). Polynuclear aromatic compounds, part 4. In: Bitumen, coal- tar and derived products, shale-oils and soots, vol 35, Lyon, France.

Jo, H., Noh, H., Kaviany, M., Kim, J.M., Kim, M.H. and Ahn, H.S. (2015). Tunable, self-assembled 3D reduced graphene oxide structures fabricated via boiling. *Carbon* 81: 357–366.

Lee, K.J., Miyawaki, J., Shiratori, N., Yoon, S.H. and Jang, J. (2013). Toward an effective adsorbent for polar pollutants: Formaldehyde adsorption by activated carbon. *J. Hazard. Mater.* 260: 82–88.

Li, Y., Van Zijll, M., Chiang, S. and Pan, N. (2011). KOH modified graphene nanosheets for supercapacitor electrodes. *J. Power Sources* 196: 6003–6006.

Ma, H.L., Zhang, Y.W., Hu, Q.H., Yan, D., Yu, Z.Z. and Zhai, M.L. (2012). Chemical reduction and removal of Cr(VI) from acidic aqueous solution by ethylenediamine-reduced graphene oxide. *J. Mater. Chem.* 22: 5914–5916.

Ma, J., Wang, J.N. and Wang, X.X. (2009). Large-diameter and water-dispersible single-walled carbon nanotubes: Synthesis, characterization and applications. *J. Mater. Chem.* 19: 3033–3041.

Mawhinney, D.B., Naumenko, V., Kuznetsova, A., Yates, J.T., Liu, J. and Smalley, R.E. (2000). Infrared spectral evidence for the etching of carbon nanotubes: Ozone oxidation at 298 K. *J. Am. Chem. Soc.* 122: 2383–2384.

McGwin Jr, G., Lienert, J. and Kennedy Jr, J.I. (2010). Formaldehyde exposure and asthma in children: Asystematic review. *Environ. Health Perspect.* 118: 313–317.

Paustenbach, D., Alarie, Y., Kulle, T., Schachter, N., Smith, R., Swenberg, J., Witschi, H. and Horowitz, S.B. (1997). A recommended occupational exposure limit for formaldehyde based on irritation. *J. Toxicol. Environ. Health* 50: 217–264.

Pei, J. and Zhang, J.S. (2011). On the performance and mechanisms of formaldehyde removal by chemi-sorbents. *Chem. Eng. J.* 167: 59–66.

Ramanathan, T., Fisher, F.T., Ruoff, R.S. and Brinson, L.C. (2005). Amino-functionalized carbon nanotubes for binding to polymers and biological systems. *Chem. Mater.* 17: 1290–1295.

Rong, H., Liu, Z., Wu, Q., Pan, D. and Zheng, J. (2010). Formaldehyde removal by Rayon-based activated carbon fibers modified by P-aminobenzoic acid. *Cellulose* 17: 205–214.

Salonen, H.J., Pasanen, A.L., Lappalainen, S.K., Riuttala, H.M., Tuomi, T.M., Pasanen, P.O., Bäck, B.C. and Reijula, K.E. (2009). Airborne concentrations of volatile organic compounds, formaldehyde and ammonia in Finnish office buildings with suspected indoor air problems. *J. Occup. Environ. Hyg.* 6: 200–209.

Salthammer, T., Mentese, S. and Marutzky, R. (2010). Formaldehyde in the indoor environment. *Chem. Rev.* 110: 2536–2572.

Tanada, S., Kawasaki, N., Nakamura, T., Araki, M. and Isomura, M. (1999). Removal of formaldehyde by activated carbons containing amino groups. *J. Colloid Interface Sci.* 214: 106–108.

Thommes, M., Kaneko, K., Neimark, A.V., Olivier, J.P., Rodriguez-Reinoso, F., Rouquerol, J. and Sing, K.S. (2015). Physisorption of gases, with special reference to the evaluation of surface area and pore size distribution (IUPAC Technical Report). *Pure Appl. Chem.* 87: 1051–1069.

Wu, L., Zhang, L., Meng, T., Yu, F., Chen, J. and Ma, J. (2015). Facile synthesis of 3D amino-functional graphene-sponge composites decorated by graphene nanodots with enhanced removal of indoor formaldehyde. *Aerosol Air Qual. Res.* 15: 1028–1034.

Xu, Z., Yu, J. and Xiao, W. (2013). Microemulsion-assisted preparation of a mesoporous ferrihydrite/SiO_2 composite for the efficient removal of formaldehyde from air. *Chemistry* 19: 9592–9598.

Yang, J., Li, D., Zhang, Z., Li, Q. and Wang, H. (2000). A study of the photocatalytic oxidation of formaldehyde on $Pt/Fe_2O_3/TiO_2$. *J. Photochem. Photobiol., A* 137: 197–202.

Yu, C. and Crump, D. (1998). A review of the emission of VOCs from polymeric materials used in buildings. *Build. Environ.* 33: 357–374.

Yu, F., Ma, J. and Han, S. (2014). Adsorption of tetracycline from aqueous solutions onto multi-walled carbon nanotubes with different oxygen contents. *Sci. Rep.* 4: 5326.

Zhao, D.Z., Li, X.S., Shi, C., Fan, H.Y. and Zhu, A.M. (2011). Low-concentration formaldehyde removal from air using a cycled storage–discharge (CSD) plasma catalytic process. *Chem. Eng. Sci.* 66: 3922–3929.

Received for review, July 14, 2016
Revised, December 10, 2016
Accepted, December 22, 2016